Letter

Unidirectional Perfect Reflection and Radiation in Double-Lattice Photonic Crystals

Takuya Inoue,[1,*] Naoya Noguchi,[1] Masahiro Yoshida,[2] Heungjoon Kim,[2] Takashi Asano,[2] and Susumu Noda[1,2,†]

[1] *Photonics and Electronics Science and Engineering Center, Kyoto University, Kyoto 615-8510, Japan*
[2] *Department of Electronic Science and Engineering, Kyoto University, Kyoto 615-8510, Japan*

(Received 25 January 2023; revised 31 May 2023; accepted 15 June 2023; published 7 July 2023)

Non-Hermitian photonic systems are known to exhibit unique phenomena, where non-Hermiticity is typically introduced by material loss or gain. Here, we propose and experimentally demonstrate unidirectional phenomena solely based on radiation. Our design is based on a double-lattice photonic crystal that has a linear dispersion with a single exceptional point, where the magnitudes of Hermitian and non-Hermitian couplings are canceled out in one direction. Using this concept, we realize a unidirectional waveguide that shows perfect radiation when light is incident from one side and shows perfect reflection when light is incident from the other side. Our results will open an alternative route toward harnessing non-Hermiticity.

DOI: 10.1103/PhysRevApplied.20.L011001

Non-Hermitian photonic systems, in which conservation of energy does not hold, are known to exhibit various unique optical phenomena that do not appear in the Hermitian counterpart. An important feature of non-Hermitian systems is the appearance of exceptional points (EPs) where both eigenvalues and their eigenvectors coalesce, which leads to various unique phenomena [1–10]. Unidirectional invisibility [11] and unidirectional reflectionless light propagation [12–14] are notable examples of such unique phenomena, where the reflectivity of light is strongly asymmetric depending on the direction of incidence. Unlike conventional Hermitian waveguides, where the coupling between two counterpropagating waves is bidirectional owing to the Hermiticity of the scattering matrix, non-Hermitian waveguides can realize unidirectional coupling between the two owing to their coalescence at the EP. So far, various unidirectional devices based on the introduction of absorption loss in the materials have been investigated [11–14], where the modulation of the real and imaginary parts of the permittivity causes the asymmetric wave scattering in the waveguide. However, the introduction of the material absorption loss inevitably causes the waveguided light to be absorbed unless gain is introduced, which inhibits the realization of perfect reflection and the extraction of the waveguided light for use in real applications.

In this paper, we propose a unidirectional waveguide solely based on vertical radiation from a photonic crystal, which shows perfect radiation when light comes from one side and perfect reflection when light comes from the opposite side, as shown in Fig. 1(a). Here, a double-lattice photonic crystal composed of elliptical and circular holes [15,16] is introduced in a waveguide. The origin of the unidirectionality is the Hermitian and non-Hermitian couplings between the counterpropagating waves with in-plane wave numbers of $k_x = \pm 2\pi/a$ in Figs. 1(b) and 1(c), where R_x and S_x denote the amplitudes of the basic waves. Figure 1(b) shows the Hermitian couplings without accompanying energy loss, where R and I denote the real and imaginary part of the Hermitian coupling coefficients, respectively. These coefficients are mainly determined by the Fourier coefficients that induce the second-order diffractions with reciprocal vectors of $\mathbf{G}_{\pm 2} = \pm 4\pi/a$. In double-lattice photonic crystals, R and I can be independently controlled by the hole distance (d) and the hole-size asymmetry (S_1/S_2), respectively [15,16]. On the other hand, photonic crystals with 180°-rotational symmetries (e.g., circular-hole photonic crystals [17] or rectangular gratings [18]) always satisfy $I = 0$. Figure 1(c) shows the non-Hermitian cross-couplings with radiated loss ($i\mu$), which are induced by the two-step diffraction process via the vertical radiative wave ($k_x = 0$). μ is the magnitude of the non-Hermitian coupling coefficient, determined by the Fourier coefficients that induce the first-order diffractions with reciprocal vectors of $\mathbf{G}_{\pm 1} = \pm 2\pi/a$. Using these coefficients, the eigenfrequencies near the Γ point (frequency, δ; radiation constant, α) can be analyzed with

*t_inoue@qoe.kuee.kyoto-u.ac.jp
†snoda@kuee.kyoto-u.ac.jp

coupled-wave theory [16,19] as follows:

$$(\delta + i\alpha/2)\begin{pmatrix} R_x \\ S_x \end{pmatrix} = \mathbf{C}\begin{pmatrix} R_x \\ S_x \end{pmatrix} + \begin{pmatrix} \Delta k_x R_x \\ -\Delta k_x S_x \end{pmatrix}, \quad (1)$$

$$\begin{aligned} \mathbf{C} &= \mathbf{C}_{\text{Hermitian}} + \mathbf{C}_{\text{non - Hermitian}} \\ &= \begin{pmatrix} 0 & R+iI \\ R-iI & 0 \end{pmatrix} + \begin{pmatrix} i\mu & i\mu \\ i\mu & i\mu \end{pmatrix} \\ &= \begin{pmatrix} i\mu & R+iI+i\mu \\ R-iI+i\mu & i\mu \end{pmatrix}. \end{aligned} \quad (2)$$

Here, $\mathbf{C}$ is a coupled-wave matrix, Δk_x denotes the wave number deviation from the Γ point, and δ denotes the frequency deviation from the empty lattice. $\mathbf{C}_{\text{Hermitian}}$ is a Hermitian matrix that represents the Hermitian couplings, and $\mathbf{C}_{\text{non-Hermitian}}$ is an anti-Hermitian matrix that represents the non-Hermitian couplings. The magnitude of the diagonal and nondiagonal terms in $\mathbf{C}_{\text{non-Hermitian}}$ are the same for the radiative couplings [16,19], which enables perfect reflection as explained in the following. Note that the latter becomes smaller than the former for material-loss-induced couplings without gain [12].

Figures 1(d) and 1(e) show the calculated frequencies (δ) and radiation constants (α) near the Γ point when R and I are varied and μ is fixed ($\mu = 300\ \text{cm}^{-1}$). When R is not zero (typical case), a photonic band gap (PBG) opens as shown in panels A ($I=0$) and A′ ($I\neq 0$). When both R and I are zero [17,18], the photonic band has two EPs at nonzero wave numbers as shown in panel B. As described in the previous paragraph, photonic crystals with 180°-rotational symmetries satisfy $I=0$, and they exhibit either of the photonic bands shown in panels A or B. On the other hand, the double-lattice photonic crystal can control I by changing the hole-size asymmetry (S_1/S_2), and can realize a linear dispersion with a single EP when I is equal to $\pm\mu$ as shown in panels C and D. In these cases, only one of the nondiagonal cross-coupling terms in the coupled matrix $\mathbf{C}$ in Eq. (2) (namely, $R+iI+i\mu$ or $R-iI+i\mu$) becomes zero, which realizes unidirectional scattering between the two basic waves at the EP.

More quantitatively, light propagation and vertical radiation inside the finite-sized double-lattice photonic crystal ($0 \le x \le L$, where L is the length of the waveguide) at the single EP shown in panel C ($R=0$, $I=\mu$) can be analyzed with the following coupled-wave equation [20]:

$$\frac{\partial}{\partial x}\begin{pmatrix} R_x \\ -S_x \end{pmatrix} = i\mathbf{C}\begin{pmatrix} R_x \\ S_x \end{pmatrix} = \begin{pmatrix} -\mu & -2\mu \\ 0 & -\mu \end{pmatrix}\begin{pmatrix} R_x \\ S_x \end{pmatrix}, \quad (3)$$

$$E_{\text{rad}} = \sqrt{2\mu}(R_x + S_x). \quad (4)$$

Here, E_{rad} is the electric field of the vertical radiation. By solving Eqs. (3) and (4), we can predict unidirectional reflection and radiation phenomena in the proposed device.

When R_x is incident from one side ($R_x = E_0$ at $x=0$) and L is much longer than $1/\mu$, the analytical solutions for $x>0$ are

$$\begin{aligned} R_x &= E_0 \exp(-\mu x), \quad S_x = 0, \\ E_{\text{rad}} &= \sqrt{2\mu}E_0 \exp(-\mu x). \end{aligned} \quad (5)$$

Here, all of the incident light is radiated in the vertical direction without reflection since $S_x = 0$. On the other hand, when S_x is incident from the other side ($S_x = E_0$ at $x=L$), the solutions for $x<L$ are

$$\begin{aligned} R_x &= -E_0 \exp[\mu(x-L)], \\ S_x &= E_0 \exp[\mu(x-L)], \quad E_{\text{rad}} = 0. \end{aligned} \quad (6)$$

In this case, all of the incident light is reflected backward since $|S_x| = |R_x|$ and $E_{\text{rad}}=0$. Therefore, we can realize perfect vertical radiation without reflection when light is incident from one side, and perfect reflection without radiation when light is incident from the opposite side. In the conjugate case (at the single EP shown in panel D, where $R=0$, $I=-\mu$), the incidence direction in which perfect radiation and reflection occur is reversed. Note that perfect reflection in Eq. (6) is realized only when the magnitudes of the diagonal terms and nondiagonal terms of $\mathbf{C}_{\text{non-Hermitian}}$ in Eq. (2) are balanced. When the uniform gain is provided, unidirectional invisibility [11], where light transmits through the waveguide without reflection only when the light comes from one side, can be also realized (see details in the Supplemental Material [21]).

To confirm these predictions, we perform numerical simulations of light propagation in double-lattice photonic-crystal waveguides using a three-dimensional (3D) finite-difference time-domain (FDTD) method. The lattice constant, width, thickness, and total area of the two holes are fixed to $a = 680$ nm, $w = 600$ nm, $t = 220$ nm, and $S_1 + S_2 = 0.08a^2$, respectively. In the simulations, we first investigate the structural parameters of the double-lattice photonic crystal (d and S_1/S_2) to realize photonic band structures shown in panels A–D in Fig. 1(d) (in the following, we refer to the designed structures as designs *A–D*, respectively). Then, we calculate the reflection and radiation spectra of the designed waveguides for light incident from the left and right sides. In these calculations, the light source is placed inside the coupling Si waveguides connected to the double-lattice photonic crystals, and the length L of the photonic crystal is assumed to be long enough ($320a$) to enable perfect radiation without transmission. Figure 2 shows the calculated band structures and reflection and radiation spectra for designs *A–D*. In these figures, the radiation efficiency e is calculated based on the sum of the upward and downward radiation (note that the introduction of vertical asymmetry may also

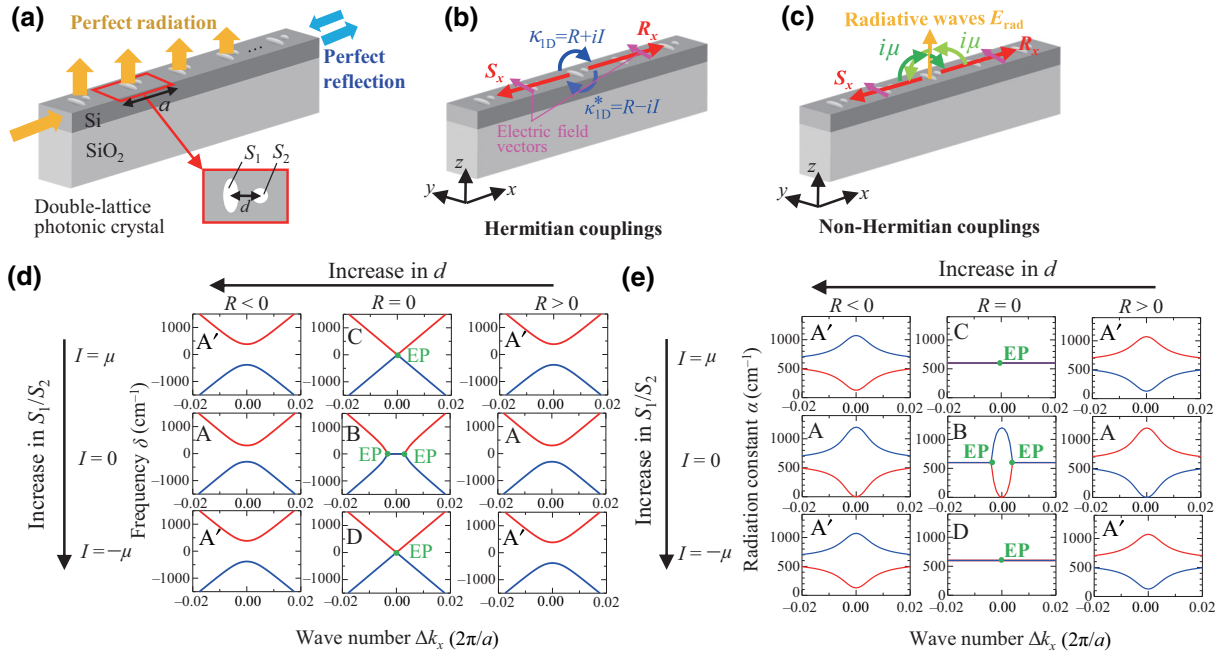

FIG. 1. (a) Schematic of a unidirectional device with a double-lattice photonic crystal. (b),(c) Hermitian and non-Hermitian cross-couplings between the basic waves. (d),(e) Calculated photonic band structures (d) and radiation constants (e) near the Γ-point when the Hermitian coupling coefficients (R and I) are varied and the non-Hermitian coupling coefficient is fixed ($\mu = 300$ cm^{-1}). Unidirectionality shown in (a) can be realized at an exceptional point (EP) in panels C and D.

enable the cancellation of the downward radiation [22,23]). Figure 2(a) shows the calculated result for design A ($R > 0$, $I \sim 0$), which has a PBG at the Γ point. The reflection (radiation) spectra become almost the same for both incident light directions owing to the symmetric couplings between the two basic waves in the coupled-wave matrix $\mathbf{C}$ ($R + iI + i\mu = R - iI + i\mu$ when $I = 0$). Design B ($R \sim 0$, $I \sim 0$), which has two EPs at the off-Γ points, also shows no dependence for the incident directions as shown in Fig. 2(b). On the other hand, designs C ($R \sim 0$, $I \sim \mu$) and D ($R \sim 0$, $I \sim -\mu$), which have linear dispersions with single EPs, exhibit totally different properties from designs A and B; in these structures, we obtain nearly perfect radiation ($e > 0.99$) for light incident from one side and nearly perfect reflection ($r > 0.99$) for light incident from the other side at the frequency of the EP. The calculated far-field pattern of the perfect radiation is a line-shaped beam with a narrow divergence angle of less than 2° (see details in the Supplemental Material [21]), which is potentially suitable for various practical applications. The dependence of the radiation and reflection characteristics on the incident direction is reversed for design C and design D. These results clearly validate our theoretical predictions in Eqs. (5) and (6). The robustness of the unidirectionality against the structural variations is discussed in the Supplemental Material [21].

Next, we fabricate the designed double-lattice photonic-crystal waveguides. A scanning microscope image of the fabricated double-lattice photonic crystal is shown in Fig. 3(a). Here, we employ a double-lattice photonic crystal composed of rectangular and square holes instead of elliptical and circular holes in Fig. 1(a) to simplify the fabrication process. The lattice constant, width, thickness, and total area of the two air holes in the fabricated structures are $a = 750$ nm, $w = 510$ nm, $t = 220$ nm, and $S_1 + S_2 = 0.094a^2$, respectively. The deviation of these parameters and the hole shape from the ones used in our simulation do not inhibit the unidirectionality of the device itself, since the unidirectionality is mainly determined by the hole distance d and the hole-size balance S_1/S_2. Here, we achieve unidirectionality by slightly increasing d in order to preserve the linear dispersion with a single EP. We fabricate two devices with different double-lattice parameters: device 1 ($d = 0.278a$, $S_1/S_2 = 1.23$) and device 2 ($d = 0.298a$, $S_1/S_2 = 1.09$). We confirm from 3D FDTD simulations that the former corresponds to design A ($R > 0$, $I \sim 0$) and the latter corresponds to design C ($R \sim 0$, $I \sim \mu$). Figure 3(b) shows an optical microscope image of the entire device, which includes two waveguides with oppositely oriented double-lattice photonic crystals to investigate the dependence on the direction of incidence.

Figure 3(c) shows a schematic of the setup for measuring radiation spectra from the double-lattice photonic crystals. Light from a wavelength-tunable laser is incident on the cleaved edge of the device using an objective lens. The radiation from the double-lattice photonic-crystal waveguide is collected by another lens and the radiative

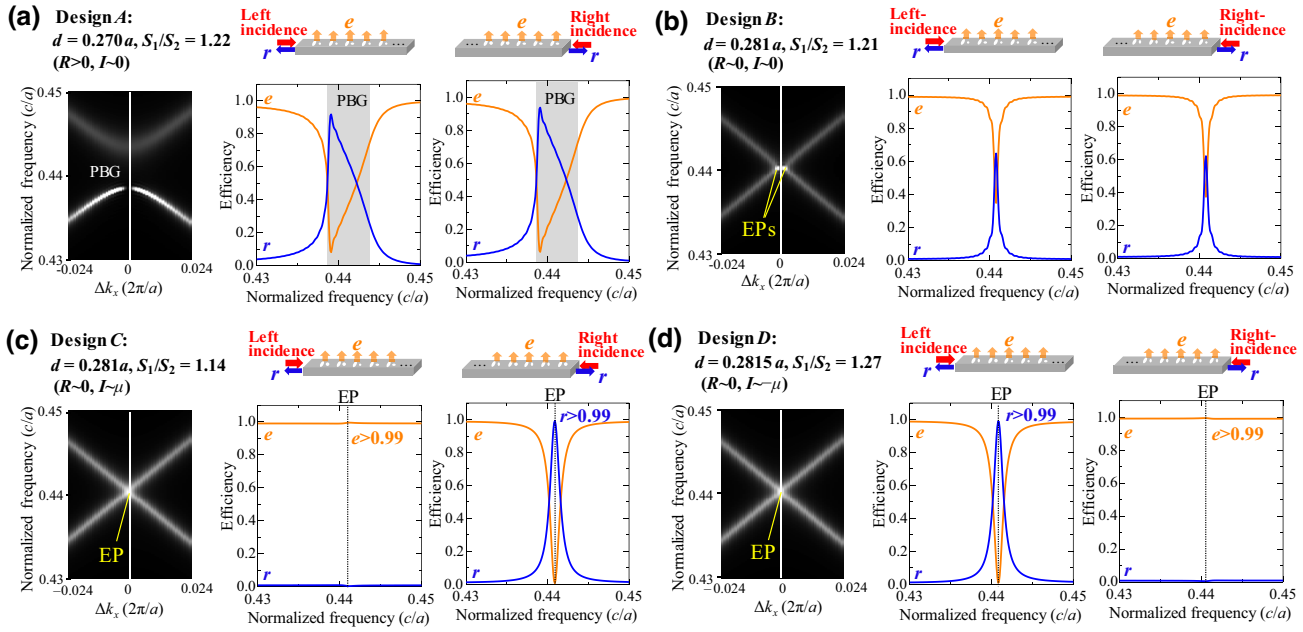

FIG. 2. Calculated band structures and reflection and radiation spectra for left-incident and right-incident light for the designed double-lattice photonic-crystal waveguides (designs *A*–*D*). Designs *C* and *D* show perfect radiation ($e > 0.99$) for light incident from one side and perfect reflection ($r > 0.99$) for light incident from the other side at the EP.

power is measured using a power meter. A mechanical chopper and a lock-in amplifier for synchronous detection are used to improve the signal-to-noise ratio. Each waveguide has a straight section without double-lattice photonic crystals ($L_{wg} = 220$ μm), as shown in Fig. 3(b), so that we can collect the radiation from the double-lattice photonic crystals separately from the scattered light at the cleaved edge. Figures 3(d) and 3(e) show the measure

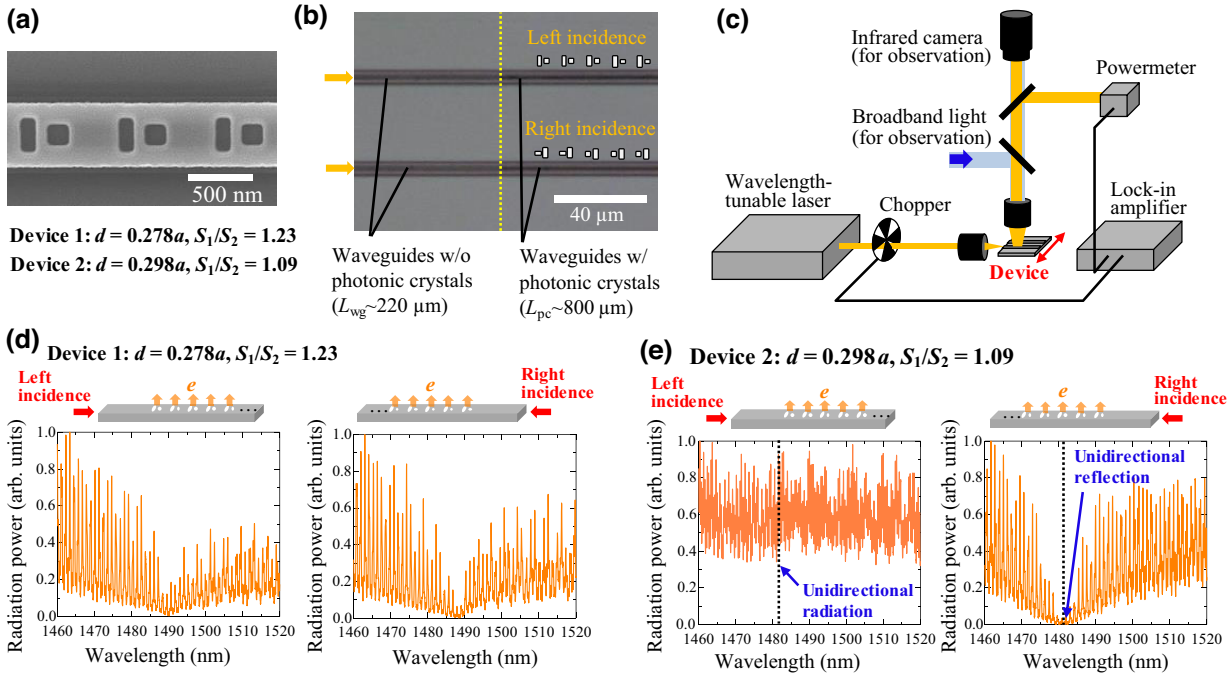

FIG. 3. (a) Scanning-electron-microscope image of a fabricated double-lattice photonic crystal. (b) Optical microscope image of the entire device. (c) Experimental setup for measuring radiation spectra. (d),(e) Measured radiation spectra of devices 1 ($R > 0$, $I \sim 0$) and 2 ($R \sim 0$, $I \sim \mu$) when the incident direction of light is reversed.

radiation spectra of devices 1 and 2 when the direction of incident light is reversed. For device 1, the radiation power is minimum around a wavelength of 1490 nm for both incident directions, which qualitatively agrees with the simulated result shown in Fig. 2(a). On the other hand, for device 2 [Fig. 3(e)], the radiation power is almost independent of the wavelength for left-incident light, while it falls to nearly zero at a wavelength of 1482 nm for right-incident light, indicating that unidirectional radiation (reflection) is achieved. In addition, we also estimate the reflectivity spectra of the fabricated double-lattice photonic crystals from the fringe patterns appearing in the radiation spectra (see details in the Supplemental Material [21]). We confirm that device 2 shows a high peak reflectivity ($r > 0.8$) around a wavelength of 1482 nm for light incident from the right and low peak reflectivities ($r < 0.1$) at all wavelengths for light incident from the left, which is further evidence of unidirectional reflection in our device.

In conclusion, we demonstrate unidirectional optical waveguides based on double-lattice photonic crystals, which show perfect vertical radiation when light is incident from one side and perfect reflection when light is incident from the opposite side. Such unidirectional characteristics are based on a linear optical dispersion with a single EP, which can be realized by balancing the Hermitian and non-Hermitian couplings inside the double-lattice photonic crystals. Unlike previously demonstrated unidirectional waveguides, our proposed devices can achieve unidirectional narrow-divergence vertical radiation of 100% of the incident light owing to the absence of material loss, and thus our devices enable various applications, such as highly efficient optical antennas for laser remote sensing and backward-reflection-free vertical couplers for silicon photonics. Our devices offer new degrees of freedom in the design of various nanophotonic devices harnessing non-Hermiticity, and they will greatly expand the utility of non-Hermitian devices in practical applications.

Acknowledgments.—We thank X. Yin and J. Gelleta for useful discussions. This work was partially supported by a Grant-in-Aid for Scientific Research (Grants No. 22H04915, No. 20H02655) from the Japan Society for the Promotion of Science (JSPS).

[1] R. El-Ganainy, K. G. Makris, M. Khajavikhan, Z. H. Musslimani, S. Rotter, and D. N. Christodoulides, Non-Hermitian physics and PT symmetry, Nat. Phys. **14**, 11 (2018).

[2] M.-A. Miri and A. Alu, Exceptional points in optics and photonics, Science **363**, eaar7709 (2019).

[3] L. Feng, Z. J. Wong, R.-M. Ma, Y. Wang, and X. Zhang, Single-mode laser by parity-time symmetry breaking, Science **346**, 972 (2014).

[4] H. Hodaei, M.-A. Miri, M. Heinrich, D. N. Christodoulides, and M. Khajavikhan, Parity-time-symmetric microring lasers, Science **346**, 975 (2014).

[5] Z. Lin, A. Pick, M. Loncar, and A. W. Rodriguez, Enhanced Spontaneous Emission at Third-Order Dirac Exceptional Points in Inverse-Designed Photonic Crystals, Phys. Rev. Lett. **117**, 107402 (2016).

[6] J. Doppler, A. A. Mailybaev, J. Bohm, U. Kuhl, A. Grischik, F. Libisch, T. J. Milburn, P. Rabl, N. Moiseyev, and S. Rotter, Dynamically encircling an exceptional point for asymmetric mode switching, Nature **537**, 76 (2016).

[7] W. Chen, S. K. Ozdemir, G. Zhao, J. Wiersig, and L. Yang, Exceptional points enhance sensing in an optical microcavity, Nature **548**, 192 (2017).

[8] T. Goldzak, A. A. Mailybaev, and N. Moiseyev, Light Stops at Exceptional Points, Phys. Rev. Lett. **120**, 013901 (2018).

[9] Y.-H. Lai, Y.-K. Lu, M.-G. Suh, Z. Yuan, and K. Vahala, Observation of the exceptional-point-enhanced Sagnac effect, Nature **576**, 65 (2019).

[10] M. P. Hokmabadi, A. Schumer, D. N. Christodoulides, and M. Khajavikhan, Non-Hermitian ring laser gyroscopes with enhanced Sagnac sensitivity, Nature **576**, 70 (2019).

[11] Z. Lin, H. Ramezani, T. Eichelkraut, T. Kottos, H. Cao, and D. N. Christodoulides, Unidirectional Invisibility Induced by PT-Symmetric Periodic Structures, Phys. Rev. Lett. **106**, 213901 (2011).

[12] L. Feng, Y.-L. Xu, W. S. Fegadolli, M.-H. Lu, J. E. B. Oliveira, V. R. Almeida, Y.-F. Chen, and A. Scherer, Experimental demonstration of a unidirectional reflectionless parity-time metamaterial at optical frequencies, Nat. Mater. **12**, 108 (2013).

[13] L. Feng, X. Zhu, S. Yang, H. Zhu, P. Zhang, X. Yin, Y. Wang, and X. Zhang, Demonstration of a large-scale optical exceptional point structure, Opt. Express **22**, 1760 (2014).

[14] Y. Huang, Y. Shen, C. Min, S. Fan, and G. Veronis, Unidirectional reflectionless light propagation at exceptional points, Nanophotonics **6**, 977 (2017).

[15] M. Yoshida, M. De Zoysa, K. Ishizaki, Y. Tanaka, M. Kawasaki, R. Hatsuda, B. Song, J. Gelleta, and S. Noda, Double-lattice photonic-crystal resonators enabling high-brightness semiconductor lasers with symmetric narrow-divergence beams, Nat. Mater. **18**, 121 (2019).

[16] T. Inoue, M. Yoshida, J. Gelleta, K. Izumi, K. Yoshida, K. Ishizaki, M. D. Zoysa, and S. Noda, General recipe to realize photonic-crystal surface-emitting lasers with 100-W-to-1-kW single-mode operation, Nat. Commun. **13**, 3262 (2022).

[17] B. Zhen, C. W. Hsu, Y. Igarashi, L. Lu, I. Kaminer, A. Pick, S.-L. Chua, J. D. Joannopoulos, and M. Soljacic, Spawning rings of exceptional points out of Dirac cones, Nature **525**, 354 (2015).

[18] A. Yulaev, S. Kim, Q. Li, D. A. Westly, B. J. Roxworthy, K. Srinivasan, and V. A. Aksyuk, Exceptional points in lossy media lead to deep polynomial wave penetration with spatially uniform power loss, Nat. Nanotechnol. **17**, 583 (2022).

[19] Y. Liang, C. Peng, K. Sakai, S. Iwahashi, and S. Noda, Three-dimensional coupled-wave model for square-lattice

photonic crystal lasers with transverse electric polarization: A general approach, Phys. Rev. B **84**, 195119 (2011).

[20] Y. Liang, C. Peng, K. Sakai, S. Iwahashi, and S. Noda, Three-dimensional coupled-wave model for square-lattice photonic crystal lasers with transverse electric polarization: Finite-size effects, Opt. Express **20**, 15945 (2012).

[21] See Supplemental Material at http://link.aps.org/supplemental/10.1103/PhysRevApplied.20.L011001 for theoretical analyses considering uniform gain; simulated results of the far-field radiation pattern; discussion on the robustness of unidirectional radiation and reflection; and details of reflectivity estimation.

[22] T. Asano, M. Mochizuki, S. Noda, M. Okano, and M. Imada, A channel drop filter using a single defect in a 2-D photonic crystal slab-defect engineering with respect to polarization mode and ratio of emissions from upper and lower sides, J. Lightwave Technol. **21**, 1370 (2003).

[23] X. Yin, J. Jin, M. Soljacic, C. Peng, and B. Chen, Observation of topologically enabled unidirectional guided resonances, Nature **580**, 467 (2020).